Biosensors and Bioelectronics 183 (2021) 113196

Contents lists available at ScienceDirect

Biosensors and Bioelectronics

journal homepage: http://www.elsevier.com/locate/bios

Aptamer assisted CRISPR-Cas12a strategy for small molecule diagnostics

Chenqi Niu [a], Chuyi Wang [a], Fan Li [a], Xiang Zheng [a], Xinhui Xing [a,b], Chong Zhang [a,b,*]

[a] MOE Key Laboratory for Industrial Biocatalysis, Institute of Biochemical Engineering, Department of Chemical Engineering, Tsinghua University, Beijing, 100084, China
[b] Center for Synthetic and Systems Biology, Tsinghua University, Beijing, 100084, China

ARTICLE INFO

Keywords:
Molecular diagnostics
ATP
CRISPR-Cas12a
Aptamer
Cleavage kinetics

ABSTRACT

Molecular diagnostics are vital for the identification, prevention, and treatment of numerous diseases and are of particular demand in point-of-care (POC) settings. Nevertheless, most reported biosensors based on the CRISPR-Cas system have focused on nucleic-acid targets. Here, we report a versatile diagnostic strategy for small molecules called Molecular Radar (Random Molecular Aptamer-Dependent CRISPR-Assist Reporter), The workflow is simple, convenient, and rapid (conducted at 37 °C in under 25 min), indicating the substantial potential of the proposed assay could be adapted into a biosensor for POC settings and on-site molecular diagnostics.

This strategy is based on the CRISPR Cas12a-assisted fluorescence reporter system that consists of Cas12a, CRISPR RNA (crRNA), a single-stranded DNA (ssDNA) probe labeled with a fluorophore at the 5′ end and a quencher at the 3' end (F-Q probe), and a single-stranded DNA aptamer for the target molecule. In the presence of a target molecule, the aptamer binds to this small molecule with high specificity and affinity, resulting in a decrease of aptamer hybridized to the crRNA-Cas12a duplex. This decrease in activated Cas12a leads to a significant reduction in fluorescence signal. In this study, adenosine-5´-triphosphate (ATP) was selected as model target molecule and an ATP detect method was developed with high specificity and sensitivity with a linear range from 25 to 500 μM and a detection limit of 104 nM. Moreover, the particular characteristics of CRISPR-Cas12a that we report here for the first time have enriched our understanding of Cas12a and provided guidance for further research on CRISPR-Cas12a-based biosensors.

1. Introduction

Molecular diagnostics are vital for the identification, prevention, and treatment of numerous diseases. Consequently, the development of efficient diagnostic tools is of critical importance (Esfandyarpour et al., 2019; Huang and Liu, 2010; Yamasaki et al., 2019). While many detection strategies with different characteristics have been reported, new diagnostic strategies that are highly sensitive, specific, rapid, and inexpensive are warranted in point-of-care (POC) settings.

Clustered Regularly Interspaced Short Palindromic Repeats (CRISPR) and CRISPR-associated proteins (Cas)—recent discoveries together referred to as the CRISPR-Cas system—have been used as efficient tools not only in genome editing (Cong et al., 2013; Jinek et al., 2012; Mali et al., 2013; Ran et al., 2013; Wang et al., 2013), but also in other fields including medical nucleic acid diagnostics (Chen et al., 2018; Gootenberg et al., 2017; Hajian et al., 2019; Li et al., 2018b; Zetsche et al., 2015; Zhou et al., 2018). Among them, SHERLOCK (Specific High-sensitivity Enzymatic Reporter UnLOCKing) (Gootenberg et al., 2017) based on CRISPR-Cas13a (C2c2) and DETECTR (DNA Endonuclease-Targeted CRISPR Trans Reporter) (Chen et al., 2018) based on CRISPR-Cas12a (Cpf1) are the classic applications for nucleic acid diagnostics. In the CRISPR-Cas12a system, the single-stranded guide CRISPR RNA (crRNA) specifically binds with the target nucleic acids to form a ternary complex (Cas12a protein, crRNA, and target nucleic acids). The Cas12a protein then shows DNase activity, which not only cleaves the target DNA, but also indiscriminately cleaves any non-target ssDNA surrounding the target DNA (Chen et al., 2018; Li et al., 2018b). The target DNA is thereby detected by monitoring the fluorescence from a non-target ssDNA florescent probe. This collateral cleavage is called *trans*-cleavage compared with *cis*-cleavage—which cleaves the target DNA—and significantly promotes the sensitivity of DNA detection. In addition, the protospacer adjacent motif (PAM) sequence ensures highly specific binding between crRNA and target nucleic acids. As a result, the CRISPR-Cas system has shown great potential, with applications in nucleic acid-related diagnostics such as human genotyping, cancer mutation testing, DNA methylation testing,

* Corresponding author. MOE Key Laboratory for Industrial Biocatalysis, Institute of Biochemical Engineering, Department of Chemical Engineering, Tsinghua University, Beijing, 100084, China.
E-mail address: chongzhang@mail.tsinghua.edu.cn (C. Zhang).

https://doi.org/10.1016/j.bios.2021.113196
Received 14 October 2020; Received in revised form 3 January 2021; Accepted 20 March 2021
Available online 24 March 2021

single nucleotide polymorphism (SNP) analysis, pathogen detection, and virus detection (Chen et al., 2018; Cheung et al., 2018; Gootenberg et al., 2017; Li et al., 2019; Myhrvold et al., 2018; Wang et al., 2020; Zhang et al., 2020). Nevertheless, most reported biosensors based on the CRISPR-Cas system have focused on nucleic-acid targets, while small-molecule CRISPR technologies have not yet been fully exploited.

Hence, it is necessary to develop more CRISPR-Cas biosensors to broaden the application range of targets beyond nucleic acids. The major challenge in developing CRISPR-Cas biosensors targeting small molecules is the transfer of small molecular signals to DNA signals that can bind to crRNA and activate the CRISPR-Cas protein to show *trans*-cleavage activity. Recently, a CRISPR-Cas12a biosensor for small molecules and double-stranded DNA based on competitive binding activities of bacterial allosteric transcription factors (aTFs) was reported (Liang et al., 2019). However, due to the limited number of target-responsive aTFs, the strategy has not been widely applied among the massive number of small-molecule targets. In addition, an ATP biosensor based on CRISPR-Cas12a was reported. However, due to the limitation of oligonucleotide design rules, it failed to achieve the best performance of Cas12a and led to mediocre detection range, LOD and detection time (Peng et al., 2020). Moreover, a CRISPR-Cas12a biosensor based on the regulation of aptamer functional DNA (fDNA) molecules has been reported (Xiong et al., 2020). The key capture probe was a sandwich-like structure including two aptamers and one locked activator; this complex probe design made it inaccessible and limited its application.

In seeking the full potential of CRISPR technologies for diagnostic applications, we were the first to report an important characteristic of CRISPR-Cas12a—namely, that a high concentration of activator (ssDNA or dsDNA that binds to crRNA) can inhibit the *trans*-cleavage activity of Cas12a. According to the new characteristic, we developed a versatile diagnostic strategy for small molecules called Molecular Radar (Random Molecular Aptamer-Dependent CRISPR-Assist Reporter) that achieved high sensitivity and specificity within a short period of time. A schematic of this Molecular Radar strategy is shown in Fig. 1. The ssDNA activator (aptamer, shown in yellow) was used as the recognition element for the small molecule of interest and the crRNA was designed to hybridize to the ssDNA activator. In the absence of a small molecule, the aptamer hybridized to the crRNA-Cas12a duplex and Cas12a was activated to show *trans*-cleavage activity. The ssDNA fluorescence-reporter probe labeled with a fluorophore and quencher pair at its two ends (denoted as the F-Q probe) was cleaved, resulting in separation of the fluorophore from the quencher, thereby producing an increase in fluorescence signal. Conversely, in the presence of small molecules, the aptamer would bind to those with high specificity and affinity, resulting in a decrease of aptamers hybridized to the crRNA-Cas12a duplex. The decrease in activated Cas12a, leading to a significant reduction in fluorescence signal, was compared with that of the positive control (PC). Given that the decrease in fluorescence signal was directly related to the decreased concentration of activated Cas12a—which in turn depended on the decreased concentration of the ssDNA activator by the small molecule target—the presence and concentration of the target can be determined by monitoring the change in fluorescence in the system. Based on the concept of Molecular Radar, we developed this platform as a universal biosensing strategy for the detection of small molecules.

2. Material and methods

2.1. Reagents

F-Q probe were purchased from Bio-lifesci (Guangzhou, China). NEB CutSmart™ buffer, LbCas12a (Cas12a), NEBuffer™ 2.1 and NEBuffer™ 3.1 were purchased from NEB (USA). crRNAs and aptamers were synthesized and purchased from Genewiz (New Jersey, USA). Nucleosides and human serum were purchased from Solarbio (Beijing, China).

2.2. Typical trans-cleavage reaction system

If not specifically described, the typical *trans*-cleavage reaction system was show below. The final concentration of components: 1X NEB CutSmart™ buffer, 200 nM F-Q probe, 5 nM LbCas12a, 5 nM crRNA, 5 nM aptamer and varying concentration of ATP as demand. Total volume of *trans*-cleavage reaction system was 80 μL.

In the positive control (PC), ATP in the above table was replaced with equal volume of deionized water. In the negative control (NC), ATP and aptamer were both replaced with equal volume deionized of water.

In the sensitivity test and real sample test, the final concentration of crRNA/Cas12a complex was 30 nM.

In real sample test, 1 mM ATP was mixed with 20% human serum in equal volume to obtain 0.5 mM ATP in 10% human serum. 0.5 mM ATP was mixed with 20% human serum in equal volume to obtain 0.25 mM ATP in 10% human serum. 100 μM ATP was mixed with 20% human serum in equal volume to obtain 50 μM ATP in 10% human serum.

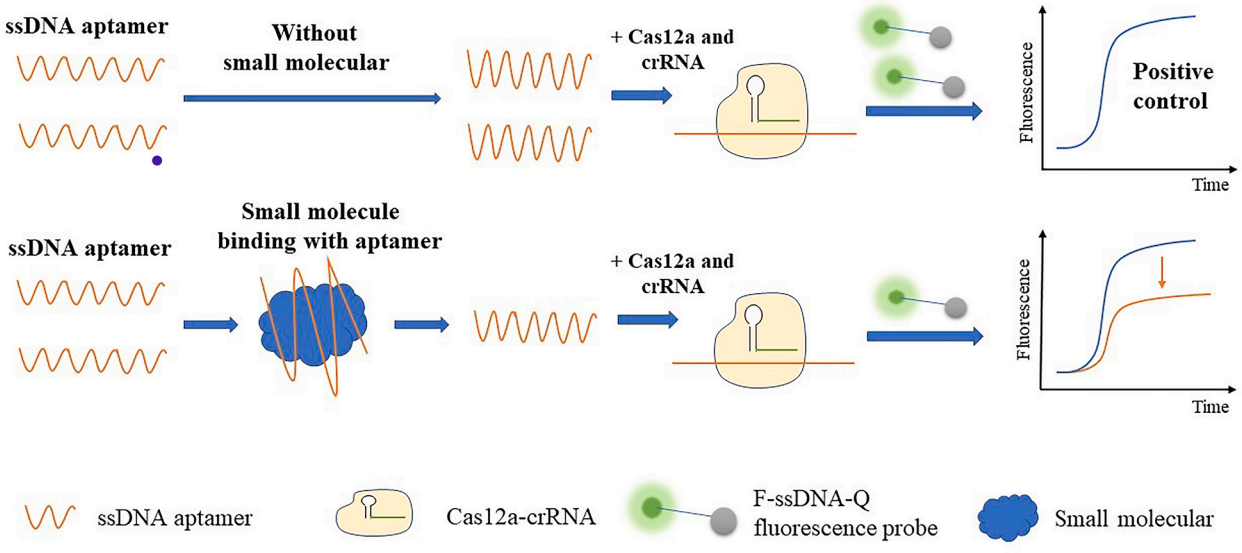

Fig. 1. Schematic of the Molecular Radar strategy for small molecules diagnostics.

2.3. Trans-cleavage assay

ATP and aptamer were incubated at room temperature for 15 min as mixture A. Meanwhile, Cas12a and crRNA were incubated at room temperature for 15 min as mixture B. After that, mixture A, mixture B, buffer, F-Q probe and deionized water were mixed evenly to start *trans*-cleavage reaction.

2.4. Data collection and processing

Reactions (80 μl, 98-well microplate format) were incubated in a fluorescence plate reader (Tecan M200 pro) for up to 60 min at 37 °C with fluorescence measurements taken every 30 s (ssDNA F-Q probe substrates = λex: 492 nm; λem: 518 nm).

GraphPad Prism 7 graphics software was used to process data and draw images. In this study, Inhibition Rate (%), IR (%) was defined to indicate the level of inhibition of *trans*-cleavage by small molecular. IR (%) = (A-B)/(A-C) × 100, where A is the fluorescence intensity in positive control, B is the fluorescence intensity in the presence of ATP, and C is the fluorescence intensity in negative control.

3. Results and discussion

3.1. Verification of the Molecular Radar

To demonstrate the feasibility of the Molecular Radar for small molecule detection, adenosine 5′-triphosphate (ATP)—the most widely used small-molecule aptamer that serves as an indicator of metabolic activity in viable cells—was selected as the model target molecule. To achieve efficient performance of the Molecular Radar strategy, the crRNA sequence design must obey the following rule: crRNA should cover as many small-molecule binding sites on the aptamer as possible, which is essential to guarantee the maximum decrease in fluorescence signal in the presence of small molecules. It has been reported that there are two ATP binding sites in the ATP aptamer (underlined G in 5′-ACCTGGGGGAGTATTGCGGAGGAAGGT-3′) (Lin and Patel 1997). The crRNA for ATP detection was designed according to this rule (Table S1) and the Molecular Radar strategy was verified using a microplate fluorescence reader. As shown in Fig. 2A, Cas12a was activated by an ATP aptamer (ssDNA activator) and showed *trans*-cleavage activity leading to a high fluorescence signal as a PC (red line). In the presence of ATP, the fluorescence signal decreased significantly, confirming that ATP led to inhibition of *trans*-cleavage activity (blue line). There are two possible reasons for this decreased signal: 1) ATP was bound with an ATP aptamer as expected in our strategy, resulting in a decrease in the

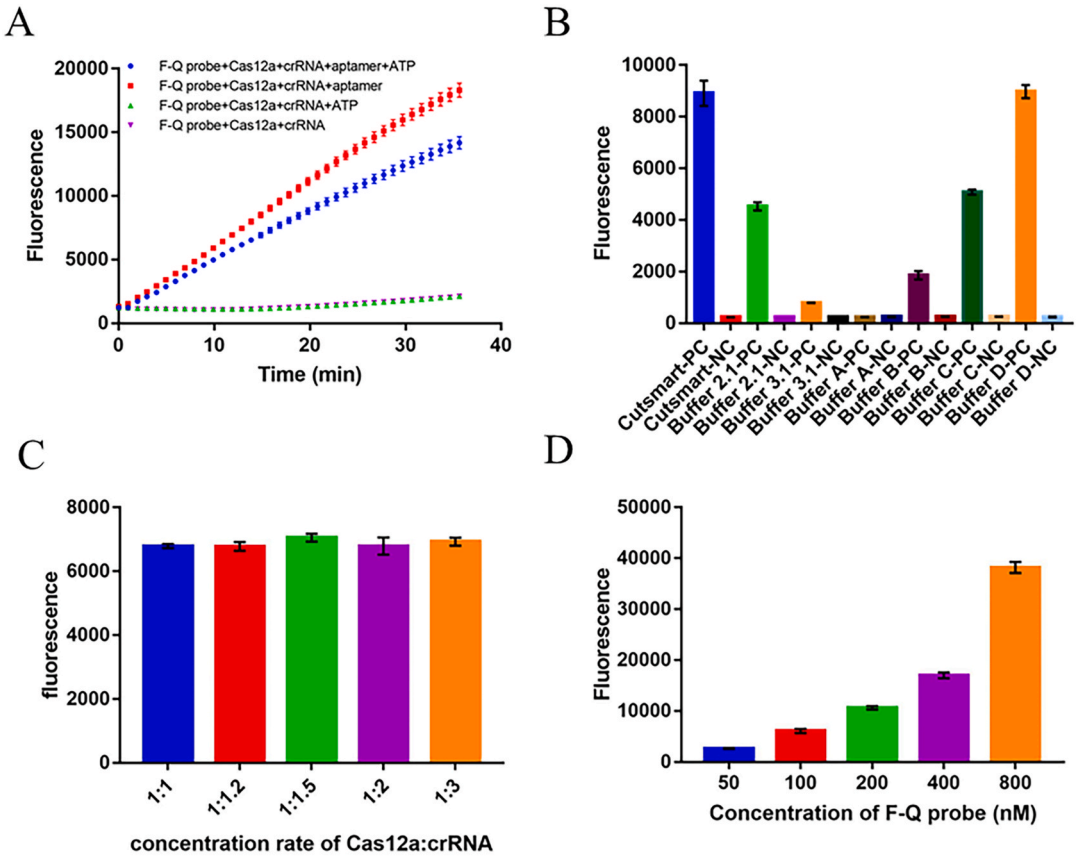

Fig. 2. Optimization of *trans*-cleavage activity in the Molecular Radar strategy for ATP detection. A) Representation of microplate fluorescence reader evaluation targeting ATP. The red line represents the positive control (PC) signal in the absence of ATP (Positive Control). The blue line represents the signal generated by the target-induced *trans*-cleavage activity of 500 μM ATP. The green line represents the background signal of 50 nM Cas12a-crRNA duplex and 500 μM ATP. The purple line represents the background signal of 50 nM Cas12a-crRNA duplex (Negative Control). B) Evaluation of the effect of the chemical environment on the *trans*-cleavage activity using 5 nM Cas12a-crRNA duplex and 25 nM ssDNA activator with fluorescence collected at 15 min. The composition of the seven buffers is shown in Table S2. C) Evaluation of the effect of the Cas12a to crRNA ratio on *trans*-cleavage activity ranging from 1:1 to 1:3 using 5 nM Cas12a and 25 nM ssDNA activator with fluorescence collected at 15 min. D) Evaluation of the effect of F-Q probe substrate concentration on the *trans*-cleavage activity using 5 nM Cas12a-crRNA duplex and 25 nM ssDNA activator with fluorescence collected at 90 min. Error bars in figures present the standard deviation (SD) based on at least three individual tests. The concentration of Cas12a-crRNA and F-Q probe is 5 nM and 200 nM respectively. PC: positive control. NC: negative control (See Material and methods for details). (For interpretation of the references to color in this figure legend, the reader is referred to the Web version of this article.)

effective ssDNA activator and a decrease in activated Cas12a; or 2) ATP inhibited cleavage activity as a universal inhibitor of protein activity. Therefore, another crRNA targeting the *EGFG* gene was designed that specifically recognized the *EGFR* gene and did not bind to ATP. The *trans*-cleavage activity activated by the *EGFR* ssDNA activator decreased negligibly in the presence of ATP compared with the significant decrease in the presence of mercury ions acting as an enzyme activity inhibitor (Figure S1). This indicated that the universal activity inhibition effect of ATP on Cas12a was excluded and the feasibility of the strategy was verified.

3.2. Evaluation of the optimized conditions for trans-cleavage

Detection sensitivity is essential for biosensing due to the lack of clinically relevant biomarkers (Azimzadeh et al., 2016; Swarts et al., 2017). The optimized conditions for *trans*-cleavage activity were evaluated to achieve the best sensitivity performance. We first investigated the Cas12a *trans*-cleavage performance in different reaction buffers (Fig. 2B). As shown, different buffers with different levels of Mg^{2+} (1 mM, 2 mM, 5 mM, 10 mM and 15 mM) led different Cas12a *trans*--cleavage activity. Cleavage activity increased with the increasing Mg^{2+} concentration in the range of 1 mM–10 mM. When the concentration of Mg^{2+} was higher than 10 mM, the cleavage activity did not increase significantly. The poorest performance with 1 mM Mg^{2+} in Buffer A indicated that Mg^{2+} concentration in the buffer was an important factor affecting Cas12a cleavage activity. The Cas12a RuvC domain is known to cleave ssDNA via the two-metal ion mechanism, in which Mg^{2+} ions induce conformational coordination of the RuvC domain and ssDNA by shifting the spatial distribution of ssDNA around the RuvC active cutting center (Dai et al., 2019; Swarts et al., 2017; Zetsche et al., 2015). In addition, Cas12a showed different *trans*-cleavage activities in NEB CutSmart™ buffer, NEBuffer™ 2.1, and NEBuffer™ 3.1 with the same Mg^{2+} concentration of 10 mM. This may result from different concentrations of anions and cations. NEBuffer™ 2.1, NEBuffer™ 3.1, NEBuffer™ 4, NEB CutSmart™ buffer, and self-made personalized buffer have been used in published studies with different *trans*-cleavage performances reported (Chen et al., 2018; Dai et al., 2019; Li et al., 2018a; Liang et al., 2019). Hence, owing to the highest fluorescence signal intensity, the NEB CutSmart™ buffer was selected as an optimized buffer for further experiments.

Efficient Cas12a-crRNA duplex concentration plays an important role in achieving satisfactory performance. In published studies, Cas12a:RNA = 1:1.25 in the DETECTR strategy (Chen et al., 2018), Cas12a:RNA = 1:2 in the HOLMES strategy (Li et al., 2018a) and Cas12a:RNA = 1:1 in the E-CRISPR strategy (Dai et al., 2019). We further investigated the ratio of Cas12a to crRNA ranging from 1:1 to 1:3. As shown in Fig. 2C, there were no significant differences in *trans*-cleavage activity at different concentration ratios, indicating that Cas12a binds to crRNA efficiently by forming a Cas12a-crRNA duplex under optimized reaction conditions. Hence—to reduce cost—the 1:1 Cas12a:RNA ratio was selected for use in the following experiments.

The concentration of Cas12a-crRNA duplex determines the number of RuvC active cutting sites and the performance of *trans*-cleavage. We further optimized the concentration of Cas12a-crRNA duplex ranging from 1 nM to 30 nM (Figure S2). The results indicated that when the concentration of Cas12a-crRNA duplex was higher than 5 nM, the reaction proceeded very quickly. At this point, the data from the PC could only be collected at the plateau stage of fluorescence increase, which was not conducive to data processing. However, when the concentration of Cas12a-crRNA duplex was lower than 5 nM, the fluorescence intensity was extremely low in the presence of ATP, making it difficult to distinguish the fluorescence intensity from the negative control (NC). Therefore, for comprehensive consideration, 5 nM Cas12a-crRNA duplex was selected for further experiments. Moreover, when compared with reports that 50 nM and 250 nM Cas12a-crRNA duplex was needed in the DETECTR and HOLMES strategies, respectively (Chen et al., 2018; Li et al., 2018a), 5 nM Cas12a-crRNA duplex used in our study significantly reduced the use of reagents, thus greatly reducing the cost.

We further evaluated the *trans*-cleavage performance in different concentrations of F-Q probe cleavage substrates ranging from 50 to 800 nM. As shown in Fig. 2D, the fluorescence intensity produced by *trans*-cleavage was proportional to the substrate concentration and the results were consistent with the kinetics of the enzyme-catalyzed reaction and the Michaelis-Menten equation. A 200 nM F-Q probe was ultimately selected for further experiments in order to distinguish the data in the presence of ATP from that in the NC, all the while taking into account cost savings.

3.3. Evaluation of the effect of activator concentration for trans-cleavage

In the Molecular Radar strategy, the aptamer activates Cas12a to perform *trans*-cleavage as a ssDNA activator. The efficient concentration of ssDNA activator decreased in the presence of ATP, leading to a decrease in fluorescence intensity. Therefore, the initial concentration of the aptamer is essential to the performance of *trans*-cleavage and detection sensitivity. We investigated the *trans*-cleavage performance of different concentrations of ssDNA activator (Fig. 3A. B). Interestingly, as shown in Fig. 3B, the fluorescence intensity did not increase as the concentration of ssDNA activator increased in all cases, instead tracing a bell curve. On the left of the peak with a low concentration of ssDNA activator, the fluorescence intensity increased with the concentration of ssDNA activator, indicating that activated Cas12a increases with the concentration of ssDNA activator. However, on the right of the peak with a high concentration of ssDNA activator, the opposite results indicated that the amount of activated Cas12a decreased. Ours is the first study to observe and demonstrate these interesting properties of Cas12a. Cas12a-crRNA-DNA triplex formation was necessary for Cas12a to perform *trans*-cleavage. It is speculated that because of the large size of Cas12a—which hinders its diffusion in the testing solution—the steric effect reduces the probability of effective collisions at a high concentration of activator, thus reducing the quantity of effectively activated Cas12a. In addition, if the activator was defined as the "activate substrate" that activated Cas12a analogous to the cleavage substrate, the bell curve indicated that excessive "activate substrate" concentration led to a decrease in enzyme activity, which is very similar to the previously reported substrate inhibition phenomenon (Cleland 1963; Gamage et al., 2003).

In order to determine whether this phenomenon only occurred when Cas12a was activated by ssDNA activation, another ssDNA activator with PAM sequence (Fig. 3C), which was a single strain from dsDNA activator for comparison with ssDNA activator without PAM sequence mentioned above and a dsDNA activator with PAM sequence (Fig. 3D) were studied. The results showed that this bell curve was also observed in both ssDNA activators with PAM sequences and dsDNA activators with PAM sequences. It is worth mentioning that the concentration ratio of Cas12a: crRNA: DNA activator was close to 1:1:1 at the peak, despite certain differences based on different sequences. For example, the maximum fluorescence intensity of ssDNA activator without PAM sequence, ssDNA activator with PAM sequence, and dsDNA activator with PAM sequence was detected at concentrations of 12.5 nM, 1 nM, and 5 nM, respectively (Fig. 3B, C, D). Furthermore, we verified this property of Cas12a via another test. When 25 nM ssDNA activator (ATP aptamer) was incubated with different concentrations of ATP ranging from 1 μM to 0.5 mM, the fluorescence signal increased compared to the PC unexpectedly with 1 μM ATP (Figure S3). A small amount of ATP bound to the aptamer resulted in an effective ssDNA activator concentration below 25 nM, making it closer to the optimal concentration (12.5 nM in Fig. 5A) and yielding better *trans*-cleavage performance. Therefore, for each *in vitro* DNA (ssDNA and dsDNA) strategy based on Cas12a, it is necessary to draw a working curve to determine the optimal concentration. The discovery of these Cas12a properties provided

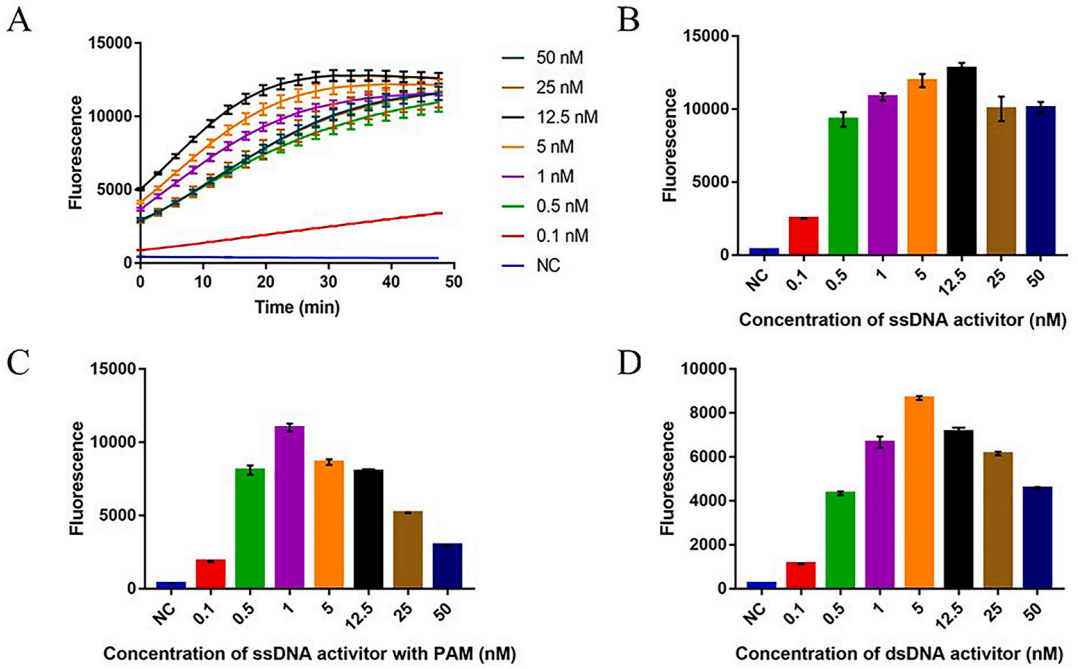

Fig. 3. Evaluation of the effect of activator concentration for *trans*-cleavage. A) *Trans*-cleavage performance with different concentrations with ssDNA activator ranging from 0.1 to 50 nM. The ssDNA activator was from the ATP aptamer. B) *Trans*-cleavage performance with different concentrations with ssDNA activator at 30 min ranging from 0.1 to 50 nM. The ssDNA activator with PAM sequence was from the ATP aptamer. C) *Trans*-cleavage performance with different concentrations with ssDNA activator with PAM sequence at 30 min ranging from 0.1 to 50 nM. The dsDNA activator was from the *EGFR* gene. D) *Trans*-cleavage performance with different concentrations with dsDNA activator with PAM sequence at 30 min ranging from 0.1 to 50 nM. The dsDNA activator was from the *EGFR* gene. Error bars in figures present the standard deviation (SD) based on at least three individual tests. The concentration of Cas12a-crRNA and F-Q probe is 5 nM and 200 nM respectively. PC: positive control. NC: negative control (See Material and methods for details).

theoretical guidance for the quantitative detection of nucleic acids based on Cas12a.

3.4. Michaelis-Menten analysis for Cas12a trans-cleavage kinetics

Michaelis-Menten analysis was completed under the optimal conditions described above. Cas12a-crRNA-ssDNA activator complexes were prepared with a final concentration of 5 nM Cas12a:5 nM crRNA:5 nM

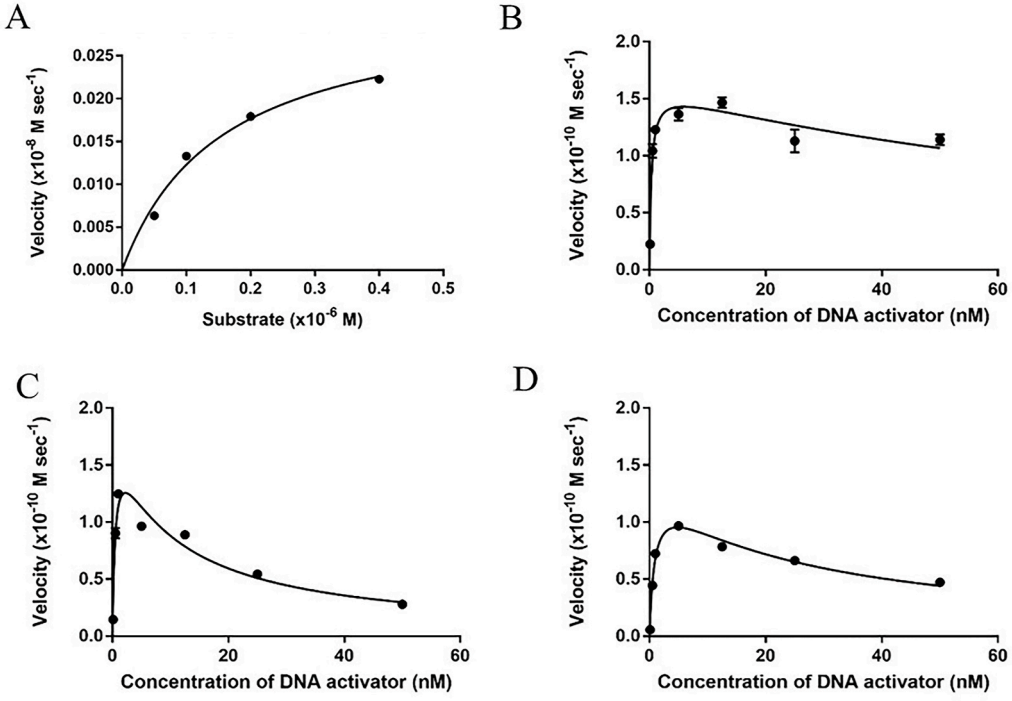

Fig. 4. Michaelis-Menten analysis for Cas12a *trans*-cleavage kinetics. A) Representative Michaelis-Menten plot for *trans* cleavage using an ssDNA activator. B) Substrate inhibition considering ssDNA activator as "activate substrate." The ssDNA activator was from the ATP aptamer. C) Substrate inhibition considering ssDNA activator with PAM sequence as "activate substrate." The ssDNA activator was from the *EGFR* gene. D) Substrate inhibition considering dsDNA activator sequence as "activate substrate." The dsDNA activator was from the *EGFR* gene. Error bars in figures present the standard deviation (SD) based on at least three individual tests. PC: positive control.

activator (effective complex = 5 nM) in a solution containing 1 × NEB CutSmart™ buffer and 50, 100, 200, 400, and 800 nM F-Q probe cleavage substrate. The initial velocity was calculated by linear regression and plotted against the substrate concentration to determine the Michaelis-Menten constants (GraphPad Software) according to the following equation: Y = (Vmax * X)/(*K*m + X), where X is the substrate concentration and Y is the enzyme velocity. The turnover number (*k*cat) was determined using the following equation: *k*cat = Vmax/Et, where Et = 5 nM. *K*m = 1.54×10^{-7} (M^{-1}), *k*cat = 6.26×10^{-2} (sec^{-1}), *k*cat/*K*m = 4.06×10^{5} (sec^{-1} M^{-1}) (Fig. 4A).

The activator was further considered as the "activate substrate." Cas12a-crRNA-DNA activator complexes were prepared at a final concentration of 5 nM Cas12a:5 nM crRNA in a solution containing × NEB CutSmart™ buffer and 200 nM F-Q probe with 0.1, 0.5, 1, 5, 12.5, 25, and 50 nM activator. The initial velocity was calculated by linear regression and plotted against the substrate concentration to determine the Michaelis-Menten constants and dissociation constant (GraphPad Software), according to the following equation: Y = Vmax * X/[*K*m + X * (1+X/Ki)]X, where X is the activator concentration and Y is the enzyme velocity. For the ssDNA activator, *K*m = 3.322×10^{-10} (M^{-1}), *K*i = 102.6×10^{-9} (M^{-1}) (Fig. 4B). For ssDNA activator with PAM sequence, *K*m = 5.114×10^{-10} (M^{-1}), *K*i = 9.718×10^{-9} (M^{-1}) (Fig. 4C). For dsDNA activator, *K*m = 9.016×10^{-10} (M^{-1}), *K*i = 25.6×10^{-9} (M^{-1}). (Fig. 4D).

3.5. Sensitivity and specificity

To determine whether the Molecular Radar strategy could detect ATP quantitatively, different concentrations of ATP were used as described in Fig. 1. Quantitative analysis was performed by monitoring the inhibition rate % (IR%) 15 min after the addition of ATP. The resulting plot of IR% vs. ATP concentrations was linear over the range of 25 μM to 0.5 mM (Fig. 5A, C). The limit of detection (LOD) was calculated to be 104 nM based on a 3*SD/slope, where SD is the standard deviation of nine NC samples. The sensitivity of our assay was comparable to those of the fluorescence biosensors reported for ATP detection (Table S3) (Helwa et al., 2012; Huang and Liu 2010; Lee et al., 2016; Liu and Lu 2006; Tedsana et al., 2013; Xiong et al. 2019). Our assay is based on the nucleic aptamer and *trans*-cleavage activity of CRISPR-Cas12a. Recognition and transformation of molecular signals are the first step of workflow: molecular signals are converted into nucleic acid signals by the specific and affinitive binding ability of aptamer. Amplification and readout of nucleic acid signals are the second step of workflow: molecular signals are converted into fluorescence signals by the *trans*-cleavage activity of CRISPR-Cas12a. In our strategy, the section of nucleic acid signal amplification and acid signal readout are combined in one step due to the *trans*-cleavage activity nuclease characteristics of Cas12a, which is simple and convenient compared to other DNA and RNA-based hybridization assays for small molecules. Moreover, more than one of units' fluorescence signal increase are led by per unit nucleic signal due to the *trans*-cleavage activity. This ensures the high sensitivity of our assay. The sensitivity is also comparable to that of commercial colorimetric/fluorometric ATP kits (LOD ≈ 1 μM) (Xiong et al. 2019).

To investigate the selectivity of the Molecular Radar strategy, different competing nucleotide-triphosphate analogs including TTP, CTP, GTP, and UTP and AMP, ADP were tested. As shown in Fig. 5B, compared with the PC samples, the fluorescence signal of 100 μM ATP showed a sharp decrease ($p < 0.0001$), while no significant differences in fluorescence signals were observed for competing analogs at a concentration of 100 μM ($p > 0.05$), suggesting that high selectivity of ATP was achieved for this strategy.

To verify the feasibility of Molecular Radar in real samples, ATP was detected in human serum (Fig. 6A). By spiking with different concentrations of ATP in 10% human serum, the recovery of the strategy was tested and the matrix effect was investigated (Fig. 6B and C). The

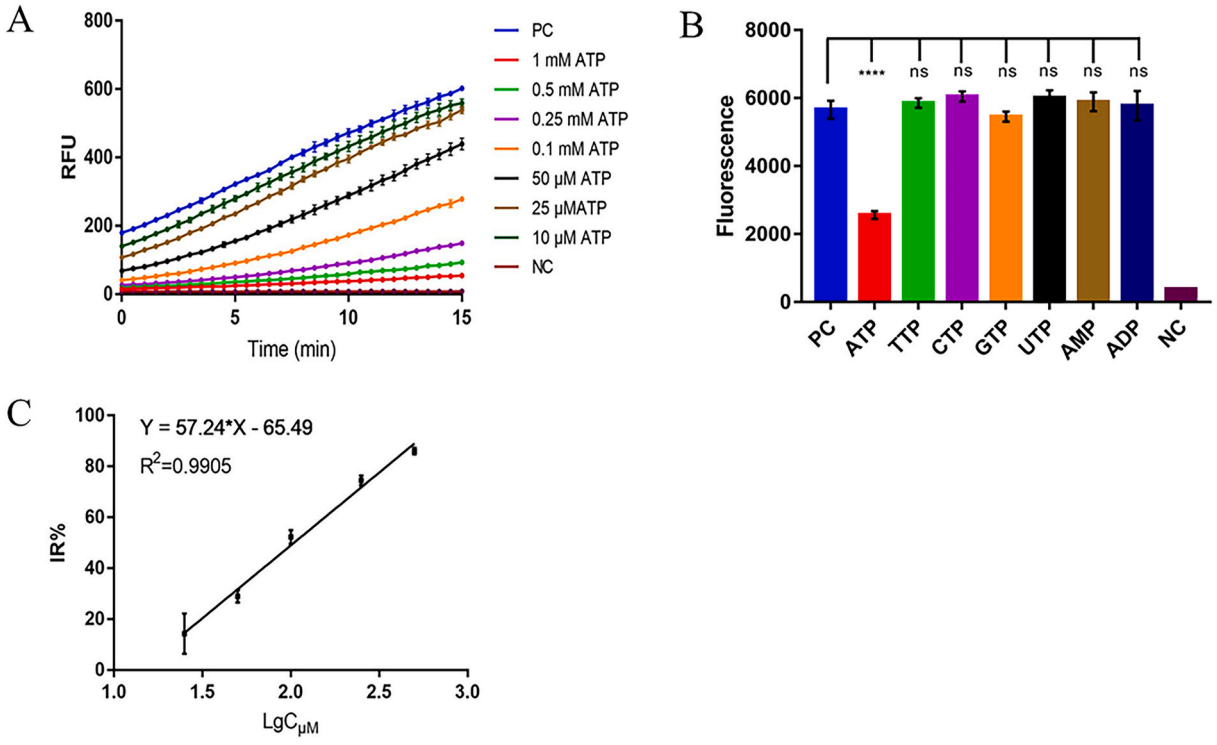

Fig. 5. The performance of the Molecular Radar. A) Kinetics of the fluorescence change at various concentrations of ATP. Inset: Linear calibration curve. B) Specificity with 100 μM nucleoside detection. C) Linear calibration curve regressed from the data in A). The data were obtained from nine independent measurements in A) and three independent measurements in B). The error bars indicate the standard deviation. ****: $P < 0.0001$. ns: no significant difference. PC: positive control. NC: negative control (See Material and methods for details).

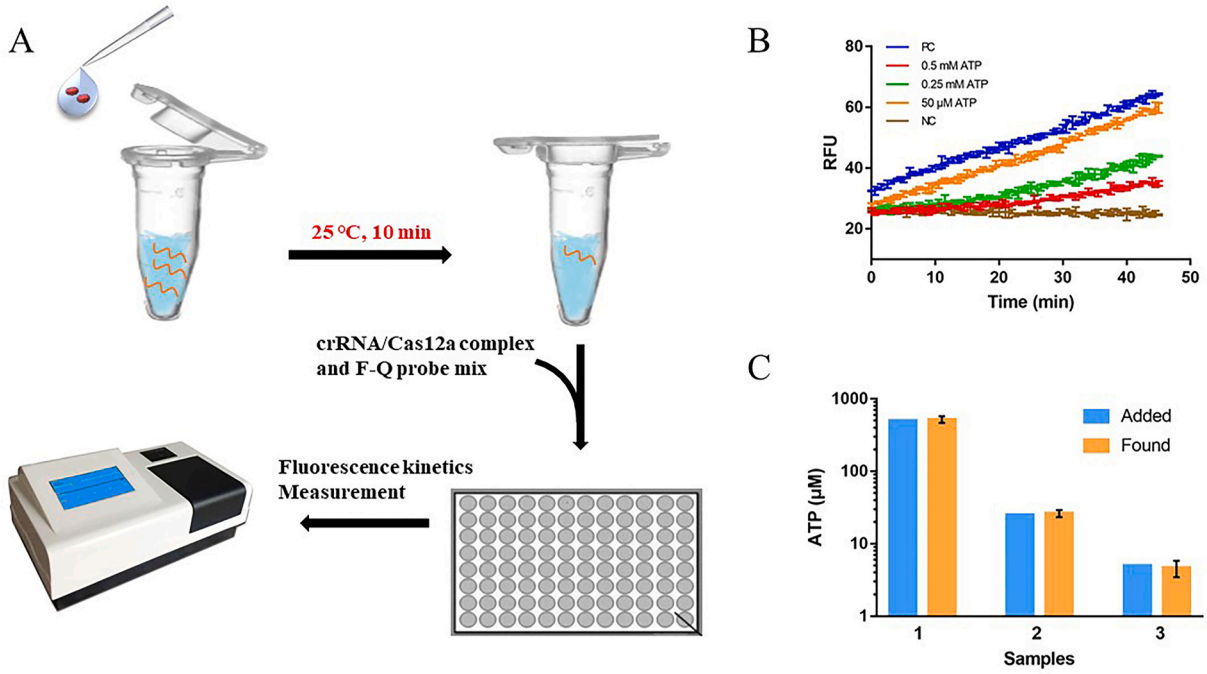

Fig. 6. Rapid detection of ATP in human serum by our Molecular Radar strategy. A) Workflow for ATP detection in 25 min. B) Fluorescence signal varied with different concentrations of ATP spiked in 10% human serum. C) Comparison of the detection results with spiked concentrations of ATP. Error bars in figures present the standard deviation (SD) based on at least three individual tests. PC: positive control. NC: negative control (See Material and methods for details).

estimated recoveries ranged from 93.5% to 105.4% (Table S4).

4. Conclusions

This study demonstrated a diagnostic strategy for the quantitative detection of small molecules. The strategy design is based on the CRISPR Cas12a-assisted fluorescence reporter system and a single-stranded DNA aptamer for the target molecule. The analytical parameters of the assay such as type of buffer, concentration of Cas12a-crRNA complex and ratio of Cas12a to crRNA were evaluated for an optimal *trans*-cleavage condition. Finally, ATP was quantitatively detected at 37 °C in 25 min with one simple step; effective performance was shown with high sensitivity and specificity, suggesting potential applications of this strategy in POC diagnostics and field tests. Moreover, given that aptamers can bind *in vitro* to a wide range of targets—from small organic molecules and metal ions to proteins and even viruses and cells—the universality of our strategy was established. It can detect not only small molecules, but can also expand the target range. Any target with the corresponding aptamer can be included. Furthermore, by changing the F-Q probe to MB-ssDNA reporter modified on the electrode, our aptamer-based strategy can be applied to electrochemical biosensors to extend the application areas and achieve higher sensitivity. In addition, we were the first to report the specific CRISPR-Cas12a characteristic that high concentrations of activators can inhibit the trans-cleavage activity of Cas12a, with Michaelis-Menten analysis for Cas12a trans-cleavage kinetics performed to obtain certain critical parameters. Overall, this novel characteristic enriches our understanding of Cas12a and provides guidance for further research on CRISPR-Cas12a-based biosensors. And the strategy revealed here provide a platform could be adapted into a biosensor for POC and on-site diagnostics, broadening the applications of the CRISPR-Cas system in biochemistry and biomedical fields.

CRediT authorship contribution statement

Chenqi Niu: Conceptualization, Formal analysis, Validation, Investigation, Writing – original draft, Writing – review & editing. **Chuyi Wang:** Formal analysis, Validation, Investigation. **Fan Li:** Formal analysis, Investigation. **Xiang Zheng:** Formal analysis, Investigation. **Xinhui Xing:** Conceptualization, Supervision, Resources.

Declaration of competing interest

The authors declare that they have no known competing financial interests or personal relationships that could have appeared to influence the work reported in this paper.

Acknowledge

This work was financially supported by the National Key Research and Development Program of China (Grant No. 2019YFA0904800) and the Foshan-Tsinghua Innovation Special Fund (FTISF) (Grant No. 2019THFS0129).

Appendix A. Supplementary data

Supplementary data to this article can be found online at https://doi.org/10.1016/j.bios.2021.113196.

References

Azimzadeh, M., Rahaie, M., Nasirizadeh, N., Ashtari, K., Naderi-Manesh, H., 2016. Biosens. Bioelectron. 77, 99–106.
Chen, J.S., Ma, E., Harrington, L.B., Da Costa, M., Tian, X., Palefsky, J.M., Doudna, J.A., 2018. Science 360 (6387), 436.
Cheung, A.H.K., Chow, C., Zhang, J.L., Zhou, Y.H., Huang, T.T., Ng, K.C.K., Or, T.C.T., Yao, Y.Y., Dong, Y.J., Fung, J.M.W., Xiong, L., Chan, A.K.Y., Lung, W.M.R., Kang, W., To, K.F., 2018. Lab. Invest. 98 (7), 968–976.
Cleland, W.W., 1963. Biochim. Biophys. Acta (BBA) - Spec. Sect. Enzymol. Subj. 67, 173–187.
Cong, L., Ran, F.A., Cox, D., Lin, S.L., Barretto, R., Habib, N., Hsu, P.D., Wu, X.B., Jiang, W.Y., Marraffini, L.A., Zhang, F., 2013. Science 339 (6121), 819–823.
Dai, Y.F., Somoza, R.A., Wang, L., Welter, J.F., Li, Y., Caplan, A.I., Liu, C.C., 2019. Angew. Chem. Int. Ed. 58 (48), 17399–17405.
Esfandyarpour, R., Kashi, A., Nemat-Gorgani, M., Wilhelmy, J., Davis, R.W., 2019. Proc. Natl. Acad. Sci. U. S. A. 116 (21), 10250–10257.

Gamage, N.U., Duggleby, R.G., Barnett, A.C., Tresillian, M., Latham, C.F., Liyou, N.E., McManus, M.E., Martin, J.L., 2003. J. Biol. Chem. 278 (9), 7655–7662.
Gootenberg, J.S., Abudayyeh, O.O., Lee, J.W., Essletzbichler, P., Dy, A.J., Joung, J., Verdine, V., Donghia, N., Daringer, N.M., Freije, C.A., Myhrvold, C., Bhattacharyya, R.P., Livny, J., Regev, A., Koonin, E.V., Hung, D.T., Sabeti, P.C., Collins, J.J., Zhang, F., 2017. Science 356 (6336), 438.
Hajian, R., Balderston, S., Tran, T., DeBoer, T., Etienne, J., Sandhu, M., Wauford, N.A., Chung, J.Y., Nokes, J., Athaiya, M., Paredes, J., Peytavi, R., Goldsmith, B., Murthy, N., Conboy, I.M., Aran, K., 2019. Nat. Biomed. Eng. 3 (6), 427–437.
Helwa, Y., Dave, N., Froidevaux, R., Samadi, A., Liu, J., 2012. ACS Appl. Mater. Interfaces 4 (4), 2228–2233.
Huang, P.-J.J., Liu, J., 2010. Anal. Chem. 82 (10), 4020–4026.
Jinek, M., Chylinski, K., Fonfara, I., Hauer, M., Doudna, J.A., Charpentier, E., 2012. Science 337 (6096), 816–821.
Lee, Y.-N., Okumura, K., Iwata, T., Takahashi, K., Hattori, T., Ishida, M., Sawada, K., 2016. Talanta 161, 419–424.
Li, L.X., Li, S.Y., Wu, N., Wu, J.C., Wang, G., Zhao, G.P., Wang, J., 2019. ACS Synth. Biol. 8 (10), 2228–2237.
Li, S.-Y., Cheng, Q.-X., Wang, J.-M., Li, X.-Y., Zhang, Z.-L., Gao, S., Cao, R.-B., Zhao, G.-P., Wang, J., 2018a. Cell Discov 4 (1), 20.
Li, S.Y., Cheng, Q.X., Liu, J.K., Nie, X.Q., Zhao, G.P., Wang, J., 2018b. Cell Res. 28 (4), 491–493.
Liang, M., Li, Z., Wang, W., Liu, J., Liu, L., Zhu, G., Karthik, L., Wang, M., Wang, K.-F., Wang, Z., Yu, J., Shuai, Y., Yu, J., Zhang, L., Yang, Z., Li, C., Zhang, Q., Shi, T., Zhou, L., Xie, F., Dai, H., Liu, X., Zhang, J., Liu, G., Zhuo, Y., Zhang, B., Liu, C., Li, S., Xia, X., Tong, Y., Liu, Y., Alterovitz, G., Tan, G.-Y., Zhang, L.-X., 2019. Nat. Commun. 10 (1), 3672.
Lin, C.H., Patel, D.J., 1997. Chem. Biol. 4 (11), 817–832.
Liu, J., Lu, Y., 2006. Angew. Chem. Int. Ed. 45 (1), 90–94.
Mali, P., Yang, L.H., Esvelt, K.M., Aach, J., Guell, M., DiCarlo, J.E., Norville, J.E., Church, G.M., 2013. Science 339 (6121), 823–826.
Myhrvold, C., Freije, C.A., Gootenberg, J.S., Abudayyeh, O.O., Metsky, H.C., Durbin, A. F., Kellner, M.J., Tan, A.L., Paul, L.M., Parham, L.A., Garcia, K.F., Barnes, K.G., Chak, B., Mondini, A., Nogueira, M.L., Isern, S., Michael, S.F., Lorenzana, I., Yozwiak, N.L., MacInnis, B.L., Bosch, I., Gehrke, L., Zhang, F., Sabeti, P.C., 2018. Science 360 (6387), 444–448.
Peng, L., Zhou, J., Liu, G., Yin, L., Ren, S., Man, S., Ma, L.J.S., 2020. Chemical, A.B., 128164
Ran, F.A., Hsu, P.D., Wright, J., Agarwala, V., Scott, D.A., Zhang, F., 2013. Nat. Protoc. 8 (11), 2281–2308.
Swarts, D.C., van der Oost, J., Jinek, M., 2017. Mol. Cell 66 (2), 221–233 e224.
Tedsana, W., Tuntulani, T., Ngeontae, W., 2013. Anal. Chim. Acta 783, 65–73.
Wang, H.Y., Yang, H., Shivalila, C.S., Dawlaty, M.M., Cheng, A.W., Zhang, F., Jaenisch, R., 2013. Cell 153 (4), 910–918.
Wang, X., Ji, P., Fan, H., Dang, L., Wan, W., Liu, S., Li, Y., Yu, W., Li, X., Ma, X., Ma, X., Zhao, Q., Huang, X., Liao, M., 2020. Commun. Biol. 3 (1), 62-62.
Xiong, Y., Zhang, J.J., Yang, Z.L., Mou, Q.B., Ma, Y., Xiong, Y.H., Lu, Y., 2020. J. Am. Chem. Soc. 142 (1), 207–213.
Yamasaki, T.R., Holmes, B.B., Furman, J.L., Dhavale, D.D., Su, B.W., Song, E.S., Cairns, N.J., Kotzbauer, P.T., Diamond, M.I., 2019. J. Biol. Chem. 294 (3), 1045–1058.
Zetsche, B., Gootenberg, J.S., Abudayyeh, O.O., Slaymaker, I.M., Makarova, K.S., Essletzbichler, P., Volz, S.E., Joung, J., van der Oost, J., Regev, A., Koonin, E.V., Zhang, F., 2015. Cell 163 (3), 759–771.
Zhang, Y.-m., Zhang, Y., Xie, K., 2020. Mol. Breed. 40 (1), 11.
Zhou, W., Hu, L., Ying, L., Zhao, Z., Chu, P.K., Yu, X.-F., 2018. Nat. Commun. 9 (1), 5012.